Grazing Incidence Diffraction and X-ray Reflectivity Studies of the Interactions of Inorganic Mercury Salts with Membrane Lipids in Langmuir Monolayers at the Air/Water Interface

Marcin Broniatowski,*,† Michał Flasiński,† Patrycja Dynarowicz-Łątka,† and Jarosław Majewski‡

Faculty of Chemistry, Jagiellonian University, Ingardena 3, 30-060 Kraków, Poland and Lujan Neutron Scattering Center, Los Alamos National Laboratory, Los Alamos, New Mexico 87545

Received: February 24, 2010; Revised Manuscript Received: June 17, 2010

The interactions of mercury ions with the membrane phospholipids are considered to be of great importance regarding the toxicity of this metal in living organisms. To obtain deeper insight into this problem, we performed systematic studies applying the Langmuir technique complemented with synchrotron X-ray scattering methods (grazing incidence X-ray diffraction (GIXD) and X-ray reflectivity (XR)). We focused our attention on the interactions of inorganic mercury salts dissolved in the aqueous subphase with lipid monolayers, formed by selected membrane phospholipids, namely, dipalmitoylphosphatidylglicerol (DPPG), dipalmitoylphosphatidylcholine (DPPC), 1-octadecyl 2-sn-phosphatidylcholine (lyso-PC), and sphingomyelin (SM). Two different inorganic mercury salts, one of a hydracid, $HgCl_2$, and the other of an oxacid, $Hg(NO_3)_2$, have been investigated. Our results proved that the elastic properties of phospholipid monolayers are a key factor regarding the interactions with mercury ions. Significant differences in mercury ions complexation are observed with double-chain phospholipids (such as DPPG and DPPC) forming fluid layers of low compressibility and phospholipids forming more compressible films (like SM and lyso-PC). Namely, important changes in the monolayer characteristic were observed only for the latter kind of lipids. This is an important finding taking into account the accumulation of mercury in the central nervous system and its neurotoxic effects. SM is one of the most abundant lipids in neurons shells and therefore can be considered as a target lipid complexing mercury ions.

Introduction

Mercury, the only liquid metal at room temperature, is known to be one of the most serious environmental pollutants. Combustion of carbon-containing mercury sulfide in large power plants, emissions of the transition and heavy metal smelters, as well as application of mercury amalgams in the metallurgy of noble metals are the main sources of the mercury vapors and methylmercury compounds in the atmosphere.[1,2] The main factors causing the direct hazard of mercury intoxication to humans are, according to the WHO, fish consumption, dental amalgams, and mercury-containing vaccine preservatives.[3,4] The acute and chronic effects of mercury intoxication are well known, and their description can be found in any handbook of toxicology.[5] Problems appear when the mechanism of mercury intoxication at the cellular level is concerned. Generally it is believed that, because of its significant affinity to the thiol (−SH) group, it binds nonspecifically to different proteins, changing and disabling their functions, which, in consequence, can lead to different dysfunctions of the cells, including their apoptosis, and, on a larger scale, to pathological changes in the target organs.[6,7] This, however, is an oversimplification, as mercury also interacts with other functional groups. For example, its affinity to nucleic bases is responsible for the Hg-caused carcinogenesis.[8]

Mercury can enter the organism in three different forms: as organometallic mercury salts (mainly methylmercury), inorganic mercury(II) salts, or mercury vapors. In fact, the two last groups can be treated jointly, as mercury vapors are oxidized in the organism to inorganic mercury salts. Therefore, all the mercury forms, when they enter the blood, are complexed with −SH group bearing compounds, such as glutathione, free cysteine, or blood albumins, and distributed in the organism.[9] Therefore, the first cells that meet mercury are erythrocytes. Mercury binds to their cellular membrane, mainly to the phospholipids of the outer leaflet (however, it can also reach the inner leaflet), leading to the change of the erythrocyte shape and various dysfunctions.[10−12] Reaching different target cells, mercury first has to penetrate the cellular membrane barrier; therefore, the interactions with cellular membrane components can be of great importance regarding the molecular mechanism of mercury toxicity.

It was proved that mercury can bind to the polar headgroups of some membrane lipids and form stable complexes.[10,13−15] The complexation of mercury ions changes the organization of the phospholipids bilayer, leading to rigidification, increasing disorder in the lateral lipid organization, and significant permeation of the membranes.[13] The primary effects are followed by other deleterious changes within the lipid bilayer. The presence of mercury ions complexed by the phospholipids headgroups activates phospholipases, especially the phospholipase A2, leading to hydrolysis of the membrane phospholipids and liberation of phospholipids degradation products.[16,17] The complexation of mercury by the headgroups activates, apart from phospholipases, other enzymes also, like catalases and peroxidases, causing the generation of reactive oxygen species and oxidative stress.[16,18,19] The products of lipid degradation, such

* To whom correspondence should be addressed. Phone: +48126632082. Fax: +48126340515. E-mail: broniato@chemia.uj.edu.pl.
† Jagiellonian University.
‡ Los Alamos National Laboratory.

10.1021/jp101668n
Published on Web 07/06/2010

SCHEME 1: Structural Formulas of the Investigated Lipids

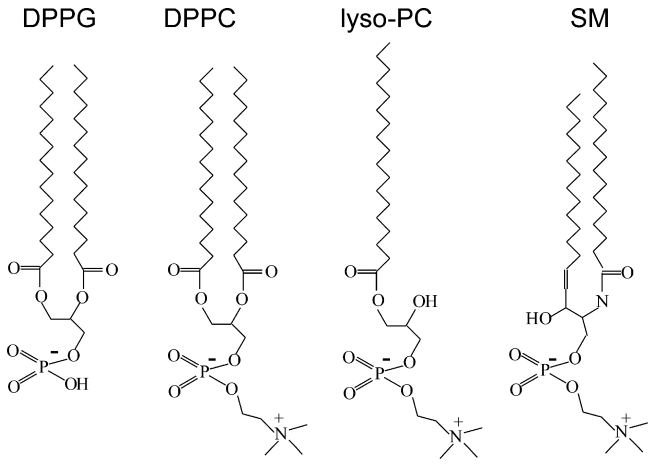

as, for example, arachidonic acid, activate different metabolic cascades, leading to inflammation and autoimmune effects.[17,20]

The interactions of inorganic mercury salts with phospholipids were investigated on living organisms,[21] isolated cell lines,[22] as well as lipid vesicles in aqueous solution.[10,13] Some studies were performed to check the affinity of the polar headgroups of membrane phospholipids toward inorganic mercury salts complexation.[13] According to these studies, Hg^{2+} binds preferentially to negatively charged phospholipids, like phosphatidyloserines (PS); however, zwitterionic phospholipids, such as phosphatidyl ethanolamines (PE) or phosphatidylcholines (PC), can also complex Hg^{2+}.

Langmuir phospholipids monolayers are very effective models of cellular membranes since their composition and organization can be strictly controlled and numerous modern physicochemical experimental methods can be applied for their investigation.[23,24] However, to the best of our knowledge, this effective model has never been applied for systematic studies of the interaction of lipid layers with mercury inorganic salts dissolved in the aqueous subphase. To fulfill this gap and shed new light on the problem of the deleterious effects exerted by mercury inorganic salts on phospholipids membranes, we performed research concerning the effects of inorganic mercury salts on the Langmuir monolayers formed by selected membrane phospholipids.

In our experiments, the following four membrane phospholipids were investigated: dipalmitoylphosphatidylglicerol (DPPG), dipalmitoylphosphatidylcholine (DPPC), 1-octadecyl 2-*sn*-phosphatidylcholine (lyso-PC), and sphingomyelin (SM). DPPG was chosen for having a negatively charged headgroup and differing from the other investigated lipids in the lack of the choline moiety (Scheme 1). DPPC was applied as it is considered to be the most abundant phospholipid of the outer biomembrane leaflet.[25] On the other hand, lyso-PC can be treated as a model one-chain phospholipid, being a product of the hydrolysis of the double-chain molecule performed by the phospholipase A2. SM is, similarly to DPPC, an abundant component of the outer leaflets of cellular membranes. Its choice was motivated by the abundance in the myelin shields of neurons. Mercury is known to accumulate in the brain and can easily cross the blood−brain barrier.[26,27] Therefore, investigation of the SM−Hg^{2+} interactions are of special interest as it can elucidate the mechanism of the above-mentioned mercury accumulation.

In our studies the monolayers of the above-mentioned four investigated lipids were spread on the surface of either pure water or 5×10^{-4} M $HgCl_2$ or $Hg(NO_3)_2$ aqueous solutions. Two different inorganic mercury salts, one of a hydracid and the other of an oxacid, were used, since profound differences can be expected in mercury complexation, depending on the anion of the applied salt.[28] The monolayers were characterized preliminary by the surface-pressure−mean molecular area ($\pi-A$) isotherms, the characteristic of which was the first estimate of the phospholipids−mercury salt interaction. Preliminary research was followed by synchrotron X-ray scattering studies. The lateral (in the *xy* plane) organization of the investigated monolayers at the air/water interface was monitored by the grazing incidence X-ray diffraction (GIXD) method, whereas the out-of-plane structure of the monolayers was observed by X-ray reflectivity (XR) experiments. GIXD is a method which proved to be very successful in the investigation of a plethora of phospholipid films[29−32] as it provides information on the in-plane organization of lipids with nearly atomic resolution. XR is a precise method providing the profiles of the electron density distribution perpendicular to the air/water interface, a method which enables measurement of the absolute electron densities, monolayer thickness, and interfacial roughness independently of the optical refractive index of the investigated interface.[33] Application of the X-ray methods can elucidate the questions related to the membrane lipids−mercury interactions.

Experimental Section

Materials. The investigated lipids (DPPG, DPPC, SM, and lyso-PC) were purchased from Sigma and used as received. HPLC-grade chloroform and methanol as well as the mercury salts $HgCl_2$ (99%) and $Hg(NO_3)_2 \cdot H_2O$ (99%) were supplied by Aldrich. The investigated lipids were dissolved in a chloroform/methanol 9/1 mixture, forming solutions with a concentration of ca. 0.3 mM (0.2−0.3 mg/mL). The solution of the required lipid in the volatile solvent was spread on the surface of the Langmuir trough by a Hamilton microsyringe. Solutions of the two mercury salts with concentrations of 5×10^{-4} M were prepared using Milli-Q water, whose pH was ca. 5.5.

Methods. The $\pi-A$ isotherms of the investigated compounds have been registered on the NIMA 611 double-barrier trough (NIMA, Coventry, U.K.). The surface pressure was monitored continuously by a Wilhelmy electronic microbalance with an accuracy of 0.1 mN/m using filter paper made of Whatman ashless chromatographic paper as the pressure sensor. Samples of the investigated lipids were dissolved in chloroform (Aldrich, spectroscopic purity). In every experiment ca. 5×10^{16} molecules were spread in the chloroform solution by a Hamilton microsyringe on the surface of ultrapure water or on the mercury salt solution (5×10^{-4} M). At least 10 min was left for solvent evaporation; then the compression was started with a compression velocity of 20 cm^2/min (ca. 2 $Å^2$/molecule·min^{-1}) as it turned out that a compression velocity up to 50 cm^2/min does not exert adverse effects on the isotherm characteristics. All the $\pi-A$ isotherms presented in the paper are averages of at least three measurements, as the reproducibility of the isotherm data is crucial, especially for discussion of the compression modulus, calculation of which needs the differentiation of the isotherm. The subphase temperature was controlled with a Julabo water circulating bath with an accuracy of 0.1 °C. All experiments were carried out at room temperature. Room temperature is often applied in the research of different phospholipids because at higher subphase temperatures the stability of monolayers systematically decreases; moreover, the stability of monolayers is of utmost importance in the performed GIXD experiments.

X-ray scattering experiments were performed at the BW1 (undulator) beamline at the HASYLAB synchrotron source (Hamburg, Germany) using a dedicated liquid surface diffractometer[25,34,35] with an incident X-ray wavelength $\lambda \approx 1.3$ Å. A thermostatted Langmuir trough made of one block of Teflon, equipped with a movable barrier for monolayer compression, was placed in a tight container and mounted on the diffractometer. After spreading a film onto the subphase, at least 40 min was allowed for the trough container to be flushed with helium to reduce the scattering background and minimize beam damage during X-ray scans. Only then the 2D films were compressed to a surface pressure of 30 mN/m, at which the X-ray experiments were performed.

X-ray Reflectivity. To minimize the beam damage during X-ray reflectivity measurements, the monolayer sample was occasionally translated in the horizontal plane, perpendicular to the beam. This was achieved by moving the trough by 2 mm, which corresponded to a full width of the beam in the horizontal plane. Rerecording of the reflectivity curve before and after such translation afforded a check of the reproducibility.

In X-ray reflectivity, detailed information about the laterally averaged, out-of-plane, electron density distribution in a film can be obtained by modeling the deviation of the measured specular X-ray reflectivity from Fresnel's curve (R_F) obtained for an ideally sharp interface.[36,37] With identical incident (α_i) and reflected (α_f) angles, $\alpha_i = \alpha_f = \alpha$, the X-ray reflectivity curve $R(Q_z)$ can be measured by a NaI scintillation detector moving on the α_f arc. The variable Q_z is the momentum transfer defined as

$$Q_z = \frac{2\pi \sin(\alpha_i)}{\lambda}$$

where λ is the wavelength of the X-ray beam. The absolute reflectivity data were obtained by subtracting the measured background and normalizing the measured reflectivity $R(Q_z)$ with respect to the incident flux. The reflectivity data were analyzed using a kinematical approach in which the ratio between the measured reflectivity and the Fresnel reflectivity (R_F) equals the square of the absolute value of the Fourier transform of the normalized gradient of the electron density across the interface.[38]

$$R(Q_z) = R_F(Q_z)\left|\frac{1}{\rho_\infty}\int \frac{d\rho}{dz}\exp(iQ'_z z)dz\right|^2$$

By assuming that a homogeneous electron density, $\rho(z)$ is laterally averaged over the footprint of the beam, an electron density model can be built with a stack of homogeneous slabs ("boxes"). Each box is assumed to have a constant electron density and thickness. The interfaces between the boxes are smeared out using a Gaussian function with a standard deviation, σ, to account for the roughness at the boundaries due to the thermally excited capillary waves and atomic roughness of the interface.[39,40] Simulations of the reflectivity profiles were performed with the Parratt32 software package (Hahn-Meitner Institute, Berlin). In this package calculation of the optical reflectivity of X-rays was based on Parratt's recursive algorithm for stratified media using independent layers.[41] Parameters in the least-squares fitting procedure of the experimental data were the electron density and thickness of each box as well as the roughness parameters between adjacent boxes.

As far as the modeling is concerned, we decided to apply the two-slab model. In this approach the phospholipid molecule is divided into two boxes of homogeneous electron density distribution. One box contains the hydrophobic alkyl chains, whereas the second one comprises the hydrophilic headgroup together with the hydration water molecules. It should be mentioned, however, that a different approach has been proposed[33] where the headgroup box is divided into subregions. This model is rather complicated and was not often applied in the past decade. Usually, the simplest two-slab model is applied for interpretation of XR results.[42,43] In the interpretation of the XR results we tried to follow the procedure described in ref 33 to divide the headgroup on subfragments for a more precise location of the fragment complexing mercury ions. However, such an approach lead us to models which were poorer than the classical two-slab approach as far as the value of χ^2 is concerned. Therefore, we decided to use the two-slab model in the interpretation of XR results.

GIXD. Regarding the GIXD experiments, the X-ray scattering theory and liquid diffractometer used here have been described previously.[35,44] GIXD experiments were carried out to obtain lateral ordering information of the samples. The scattered intensity is measured by scanning over a range of horizontal scattering vectors Q_{xy}

$$Q_{xy} \approx \frac{4\pi}{\lambda}\sin(2\theta_{xy}/2)$$

where $2\theta_{xy}$ is the angle between the incident and diffracted beam projected on the liquid surface. The GIXD intensity distribution resulting from a powder of 2D crystallites can be represented as Bragg peaks, resolved in the Q_{xy} direction, by integrating the scattered intensity over all the channels of the position-sensitive detector, perpendicular to the interface in the Q_z direction. Conversely, the Bragg rod profiles were resolved in the Q_z direction ($Q_z = 2\pi/\sin\alpha_f$) and obtained by integrating the scattered intensity over Q_{xy} corresponding to the Bragg peak. The angular positions of the Bragg peaks determine the d spacing, $d = 2\pi/Q_{xy}$ (where Q_{xy} is the position of the maximum of the Bragg peak) for the 2D lattice. From the line width of the peaks, it is possible to determine the 2D crystalline coherence length, L_{xy}, the average distance in the direction of the reciprocal lattice vector Q_{xy}, over which the ordering extends. The intensity distribution along the Bragg rod can be analyzed to determine the magnitude and direction of the molecular tilt and the coherently scattering length (L_z) of the alkyl tail measured along the backbone.

Results and Discussion

The investigated four phospholipids were spread from their solutions at the surface of pure water and 5×10^{-4} M aqueous solutions of $Hg(NO_3)_2$ and $HgCl_2$ and characterized by the surface-pressure−mean molecular area ($\pi-A$) isotherms (Figure 1).

Figure 1a shows the data collected for DPPG. All three recorded $\pi-A$ isotherms virtually overlap and have nearly the same course and practically identical collapse pressures (π_C). Thus, it can be inferred that there is no effect of the presence of mercury salts on the DPPG monolayers. Figure 1b presents the $\pi-A$ isotherms registered for DPPC. The situation is qualitatively similar as for the previously discussed DPPG. The influence of mercury ions at a concentration of 5×10^{-4} M is practically negligible. The $\pi-A$ isotherms do not overlap; however, they are situated very close to each other, and some slight differences in the course of the isotherms can be

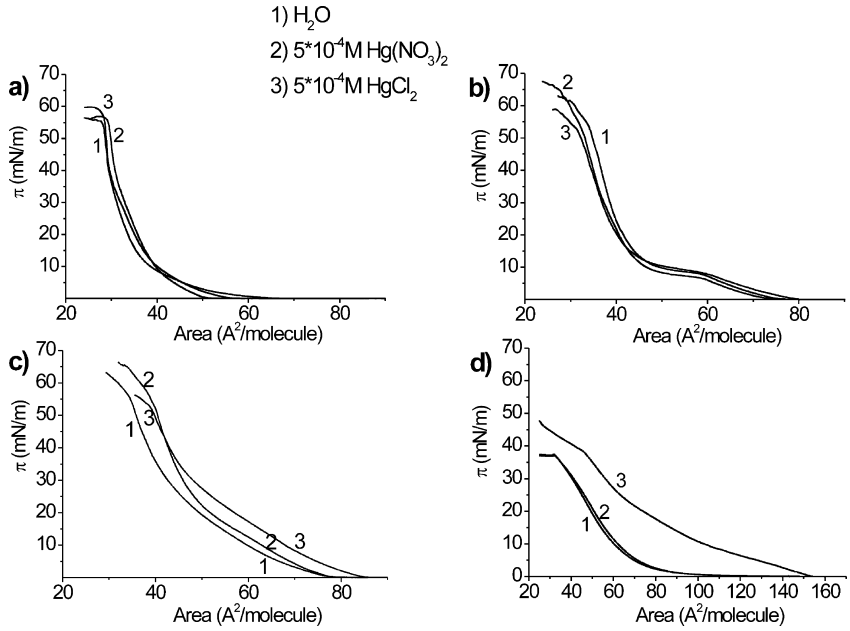

Figure 1. $\pi-A$ isotherms of the investigated lipids: (a) DPPG, (b) DPPC, (c) SM, and (d) lyso-PC on pure water (1) and the subphases containing 5×10^{-4} M $Hg(NO_3)_2$ (2) and 5×10^{-4} M $HgCl_2$ (3).

distinguished only at high surface pressures. These data imply that the effect of mercury ions on the molecular organization of DPPC in its monolayers is very weak if not negligible. $\pi-A$ isotherms collected for SM are shown in Figure 1c. The situation here is different as in the case of DPPG and DPPC. The isotherms measured on the subphase containing $Hg(NO_3)_2$ and $HgCl_2$ (10^{-4} M) solutions are shifted to higher mean molecular areas as compared to those registered on water. The shift for the $Hg(NO_3)_2$ case is small at low surface pressures but increases with the π rise. The curve measured on the subphase containing $HgCl_2$ is shifted considerably toward higher molecular areas at both low and high surface pressures. The important fact, which has to be underlined, is a greater effect of $HgCl_2$ versus $Hg(NO_3)_2$ as far as the deviation of the $\pi-A$ isotherm from the curve registered on pure water is concerned. Finally, the effect of mercury salts on lyso-PC monolayers is illustrated in Figure 1d. The isotherms measured on pure water and 10^{-4} M $Hg(NO_3)_2$ solution practically overlap, whereas the isotherm registered on $HgCl_2$ solution is profoundly shifted toward higher mean molecular areas. Here, the effect of the counterion, previously observed for SM, is much more pronounced, i.e., the mercury chloride interacts with monolayers more effectively than mercury nitrate. This effect has already been observed for one-chain surfactants, like stearic acid or octadecylamine, and is discussed in our previous paper.[28] Mercury chloride is known to be very lipophilic[45] (which is rather peculiar for an inorganic salt) and when dissolved in water dissociates to ions only on a limited scale; therefore, it can be assumed that in aqueous solution solvated $HgCl_2$ molecules, rather than solvated Hg^{2+} ions, are present. The situation is different for $Hg(NO_3)_2$ as this representative of oxacid mercury salts dissociates in water, leading to the presence of solvated Hg^{2+} cations in the aqueous subphase. Moreover, $HgCl_2$ is a salt of a strong acid and a weak base, so it can hydrolyze in water; in consequence, such complexes as $[Hg(H_2O)Cl_2OH]^-$ can be present in the solution. It is important because in such complexes the mercury atom is not a component of a positively charged moiety (as it is as a hydrated mercury cation) but forms negatively charged species. Such a negatively charged moiety tends to interact with the positively charged nitrogen atom of the choline group rather than with the partially negatively charged phosphoric acid group of a phospholipid, which distinguishes it from positively charged mercury species.

To gain more information from the $\pi-A$ isotherms, the compression moduli (C_s^{-1}) have been calculated and plotted as a function of surface pressure (see Figure 2). Compression modulus is defined according to the following formula $C_s^{-1} = -A(d\pi/dA)$ and is traditionally applied as a tool providing information on the physical state of a given monolayer.[46] It was introduced in the pioneer times of the Langmuir monolayers investigations, when the following states of the monolayers were distinguished: gaseous (G), liquid expanded (LE), liquid condensed (LC), and solid (S). C_s^{-1} higher than 12 mN/m and lower than 100 mM/m corresponds to LE, ranging from 100 to 250 mN/m to LC and higher than 250 mN/m to S.

Figure 2a shows the data calculated for DPPG. At high surface pressures C_S^{-1} exceeds 250 mN/m, but at 30 mN/m it oscillates between 100 and 200 mN/m depending on the isotherm, so for all three films their physical state can be referred to LC. For DPPC the state at 30 mN/m is S on pure water subphase and 5×10^{-4} M $Hg(NO_3)_2$, while for 5×10^{-4} M $HgCl_2$ it is LC. For SM (Figure 2c), the C_S^{-1} values at 30 mN/m range from ca. 100 mN/m on $HgCl_2$ solution to ca. 150 mN/m on pure aqueous subphase; therefore, the LC state can be ascribed to SM films. Finally, the $C_S^{-1}-\pi$ dependencies for lyso-PC do not achieve the value of 100 mN/m for any of the investigated subphases, so their state is LE. It should be underlined that according to the C_S^{-1} criterion described above, $HgCl_2$ decreases the degree of order in monolayers, as the C_S^{-1} value can qualitatively be correlated with the range of 2D crystallinity within the 2D domains (the parameter L_{xy} discussed later on); the lower the value of C_S^{-1} at a given π, the lower the range of crystallinity.

To obtain a deeper insight into the in-plane packing of the molecules at the interface and onto the out-of-plane electron density distribution of the investigated monolayers, the grazing incidence X-ray diffraction (GIXD) and X-ray reflectivity (XR) methods have been applied. If there is periodicity in a Langmuir monolayer (in-plane order), Bragg peaks and Bragg rods can be registered.[38] The interpretation of Bragg peak(s) gives the

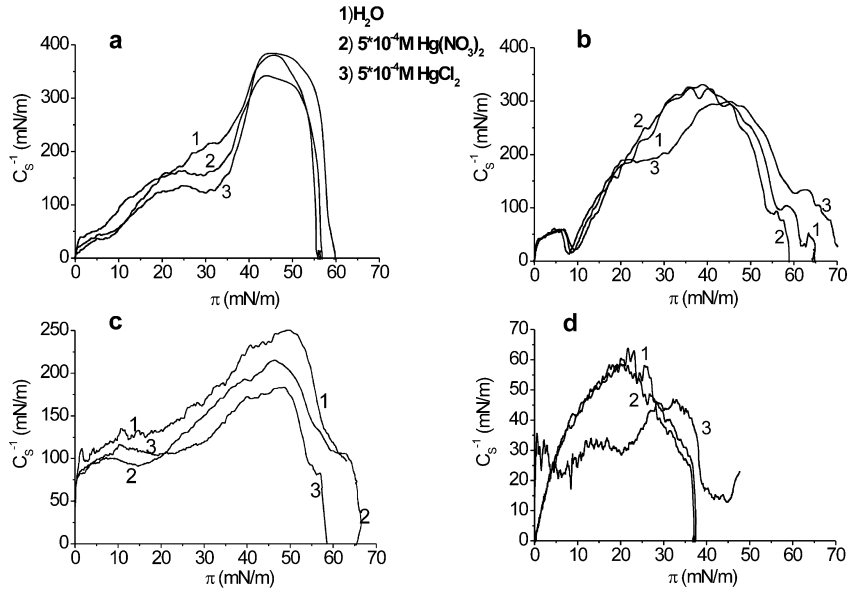

Figure 2. $C_S^{-1}-\pi$ curves calculated from the $\pi-A$ isotherms of the investigated lipids: (a) DPPG, (b) DPPC, (c) SM, and (d) lyso-PC measured on pure water (1) and the subphases containing 5×10^{-4} M $Hg(NO_3)_2$ (2) and 5×10^{-4} M $HgCl_2$ (3).

parameters of the 2D primitive unit cell (*a, b*, and γ) and the range of the crystallinity in the investigated film (the L_{xy} parameter correlated with the average size of a crystalline domain in a 2D powder). On the other hand, the interpretation of Bragg rod(s) provides information about the so-called coherence scattering length (L_z), molecular tilt, and the tilt direction. L_z is normally smaller than the geometrical length of the molecule. It is due to the fact that not the whole length of the scattering molecular part can be in registry with the other molecules. Moreover, because of thermal oscillations the terminal fragments of the hydrophobic chains are often disordered; therefore, the adjective coherent refers to the length of the fragment of the molecule, which is periodically packed in the *xy* plane.[35] In contrast to GIXD, XR does not provide information on the order within the *xy* plane but on the electron density distribution of the scattering layer perpendicular to the air/water interface. The interpretation of Bragg rods provides some information about the length of the coherently scattering molecular chain (L_z) measured along the molecular backbone, whereas the X-ray reflectivity carries information about the thickness of the monolayer, i.e., the length of the hydrophobic chain and hydrophilic head projected on the normal to the air/water interface. In the case of scattering from lipid monolayers, only XR can "see" the headgroup and is especially valuable in studying the effect of the molecules dissolved in the aqueous subphase on the organization of the monolayer at the air/water interface. In the XR experiments only intensities not phases of the radiation probe are recorded; therefore, to obtain valuable data from the $R(Q_z)$ distribution, the application of an appropriate model of electron density and successive iteration and refinement cycles are necessary.[47,48] The complexation of mercury-containing species by the phospholipids headgroups should change the order of the monolayers in the *xy* plane as well as its thickness.

In our studies we applied four different lipids. Three of them (namely, DPPC, lyso-PC, and SM; see Scheme 1) possess the same headgroup with the positively charged terminal fragment of choline. The fourth compound, DPPG, is devoid of the choline fragment and has the hydroxyl group at the third carbon atom of the glycerol backbone esterified by phosphoric acid. The headgroup of DPPG can be negatively charged due to the dissociation of the acidic hydroxyl group of the phosphoric acid residue. It is possible that the difference in the charge localized on the headgroup can significantly affect its interactions with mercury complexes; however, the experimental results do not confirm this as practically no effect of the presence of mercury salts in aqueous subphase was noticed in the course of $\pi-A$ isotherms. Therefore, DPPG was excluded from further X-ray studies, and we focused our attention on the films from DPPC, lyso-PC, and SM.

The subsequent part of our manuscript concerns the results of X-ray experiments. In the following discussion, the results from the analysis of the Bragg peaks, Bragg rods, and reflectivity curves are presented. The numeric data which can be extracted from GIXD experiments are gathered in Table 1, whereas the numeric data regarding the XR method are compiled in Table 2.

Figure 3 presents the GIXD data collected for DPPC, i.e., Bragg peaks (Figure 3a) and Bragg rods (Figure 3b) for the three investigated subphases. Relatively large values of C_S^{-1} observed for this lipid at 30 mN/m suggest a high degree of in-plane organization of the films, which is reflected in the high intensity of the diffraction peaks. In Figure 3a, two Bragg peaks are present, the first one broader, centered at 1.367 $Å^{-1}$, and the second one narrower, centered at 1.464 $Å^{-1}$. The presence of two Bragg peaks results from the distortion of the DPPC molecules from the ideal hexagonal packing, resulting in the decrease of the γ angle from 120° to 115.1°. The distortion of the hexagonal lattice originates from the collective molecular tilt of the alkyl chains of DPPC molecules. The considerable molecular tilt is reflected in the course of the Bragg rod (Figure 3b) as it has two maxima, one at the horizon (at ~0 $Å^{-1}$) and the second out of the horizon (at ~0.65 $Å^{-1}$). The analysis of the Bragg rod (through the appropriate least-squares fitting) leads to the conclusion that the molecular tilt is 30.9°, whereas the coherently scattering length (L_z) is 17.6 Å. The total length of the 15-carbon alkyl chain in its all-trans conformation, calculated with the formula $[(n - 1 + 9/8) \times 1.265]$,[35] where *n* is the number of carbon atoms, is 19.1 Å; therefore, the obtained L_z value of 17.6 Å suggests that only part of the alkyl tails are scattering coherently. The projection of the full molecular length of 19.1 Å on the *z* axis (19.1 cos(30.9°)) equals 16.4 Å and matches well the thickness of the tails box (Table 2). The in-

TABLE 1: Structural Parameters Obtained From the GIXD Data

compound	Bragg peak position ($Å^{-1}$) ± 0.0005	observed d spacing, d (Å) ± 0.0005 Å	primitive unit cell a, b, γ, (Å, Å, deg) ± 0.0005 Å; ± 0.1°	area per molecule ($Å^2$) ± 0.01 $Å^2$	coherence length L_{xy} (Å) ± 2 Å	coherence length L_z (Å) ± 0.5 Å	tilt angle, τ (deg) ±0.25°
DPPC[a]	1.367 1.464	$d_{(10,01)} = 4\ 606$ $d_{(1-1)} = 4\ 291$	$a = b$=5.085 $\gamma = 115.1$	46.82	$L_{(01,10)} = 52$ $L_{(1-1)} = 237$	16.1	30.9
SM on H_2O	1.463	4.298	$a = b = 4.961$ $\gamma = 120.0$	42.64	60	15.5	15.2
SM on 5×10^4 M $Hg(NO_3)_2$	1.412	4.458	$a = b = 5.148$ $\gamma = 120.0$	45.90	47	12.79	0
SM on 5×10^{-4} M $HgCl_2$	1.383	4.566	$a = b$= 5.273 $\gamma = 120.0$	48.15	35	10.24	0

[a] The GIXD of the DPPC on $HgCl_2$ and $Hg(NO_3)_2$ salts were identical to the case of the DPPC on pure water.

TABLE 2: Results of the XR Analysis: The Box Models of the Electron Density Distribution along the z Axis for the Investigated Monolayers Are Shown

compound	box 1 (tail)					box 2 (head)				
	length (Å)	SLD, ρ ($Å^{-2}$) × 10^{-6}	σ (Å)	e^- in box	e^- calcd	length (Å)	SLD, ρ ($Å^{-2}$) × 10^{-6}	σ (Å)	e^- in box	e^- calcd
DPPC on H_2O	15.50	9.252	4.02	242	238.1	9.08	12.09	2.76	164	182.3
SM on H_2O	15.84	9.441	4.43	226	226.1	10.94	11.94	3.17	164	184.9
SM on 5×10^{-4} M $Hg(NO_3)_2$	15.55	8.902	4.17	226	225.3	9.67	11.80	3.11	164	185.7
SM on 5×10^{-4} M $HgCl_2$	14.64	9.064	4.01	226	226.6	10.95	11.76	3.26	164	219.9
lyso-PC on H_2O	11.51	5.994	4.21	97	99.1	12.46	12.15	3.44	192	217.4
lyso-PC on 10^{-4} M $Hg(NO_3)_2$	10.71	6.056	3.96	97	93.1	12.46	12.12	3.53	192	216.9
lyso-PC on 10^{-4} M $HgCl_2$	11.51	3.880	2.90	89	89.0	11.96	13.04	3.55	200	310.8

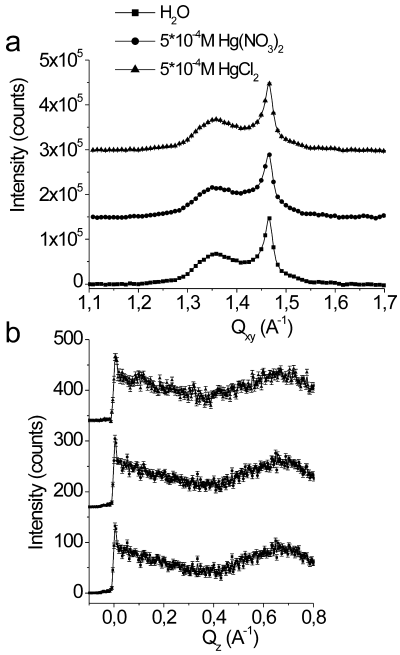

Figure 3. Background-subtracted Bragg peaks (a) and corresponding Bragg rods (b) from GIXD experiment for DPPC monolayer compressed to 30 mN/m. The Bragg rods were fitted by approximating the scattering unit of the molecule by a cylinder of constant electron density.[35] The Bragg peaks and rods measured on $Hg(NO_3)_2$ and $HgCl_2$ have been offset vertically for clarity. Due to the limited range of the position-sensitive detector the maximum value of Q_z obtained for the Bragg peaks measurements was 0.8 $Å^{-1}$.

plane coherence lengths depend on the crystallographic direction and are equal to $L_{01} = 52$ Å and $L_{11} = 237$ Å. Therefore, the 2D crystalline domain of DPPC contains approximately 1000 molecules in positional registry. Our results are consistent with previous GIXD data for DPPC, which can be found in the literature.[25,50]

As far as the interactions of the DPPC molecules with mercury salts are concerned, practically no effect can be discerned in the GIXD data; both the Bragg peaks and Bragg rods representative for the solutions of $Hg(NO_3)_2$ and $HgCl_2$ are practically identical with those registered on pure water. This suggests that the presence of these salts in the aqueous subphase does not affect the in-plane organization of the DPPC molecules.

The reflectivity curves obtained for DPPC are shown in Figure 4. The reflectivity values were multiplied by Q_z^4, and the curves were offset to obtain a better visualization of the results and highlight the possible differences between the curves. Discernible differences between the three curves in Figure 4a can be noticed at high Q_z values; however, the experimental points bear significant experimental errors. Between 0 and 0.5 $Å^{-1}$ the three registered curves are identical. To obtain information about the thickness of monolayers, the reflectivity was modeled applying the Parrat algorithm.[41] Best simple fits of the $R(Q_z)$ curve were obtained for the two-box model, i.e., the molecule was cut onto two boxes of homogeneous electron density. One of them contains the hydrophobic tail (two alkyl chains) and the second the hydrophilic headgroup. The division of the molecule is illustrated by the scheme shown in Figure 4b together with the electron density profile at the air/water interface corresponding to the applied model. According to the model, the length of the hydrophobic tail is 15.50 Å and the length of the headgroup is 9.08 Å. The length of the hydrocarbon tail corresponds well with the total length of the alkyl tails projected on the normal to the air/water interface. The length of the headgroup box corresponds well with the monocrystalline X-ray diffraction data collected for a phosphocholine group bearing lipid.[49] The number of electrons in the headgroup box exceeds by ca. 20 e^- the number of electrons in this moiety calculated from the chemical formula, suggesting that ca. 2 water molecules are hydrating the headgroup. Modeling of the reflectivity curve for the DPPC monolayers spread on the solutions of $Hg(NO_3)_2$ and $HgCl_2$ leads in the limit of the best fit (lowest χ^2) to practically

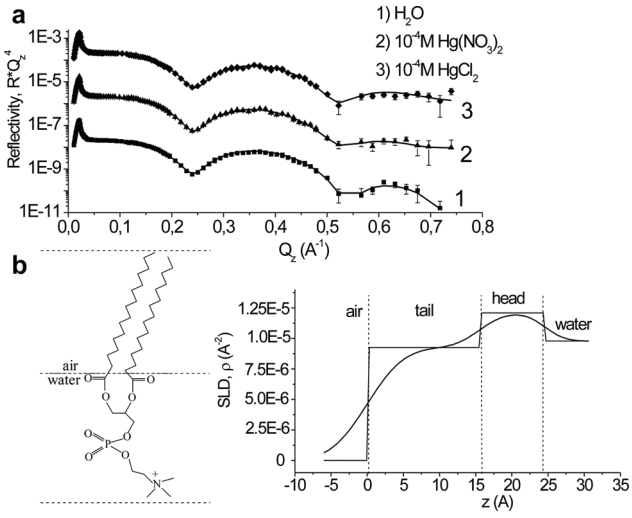

Figure 4. XR results for DPPC monolayers with and without the mercury salts. (a) XR curves for the three investigated subphases. The $R(Q_z)$ values were multiplied by Q_z^4 to underline the details of the curve course. Curves for the experiments carried out on mercury salts are offset for clarity. (b) SLD profile of the DPPC monolayer at the water/air interface. Dashed lines indicate the division of the DPPC molecule into boxes. The right-hand side of panel b shows the SLD profiles with and without roughness. The fitting parameters are summarized in Table 2.

the same model as discussed above, meaning that mercury ions are not permanently bound to the headgroups of DPPC and do not change the structural properties of the investigated films.

The GIXD data recorded for SM monolayers are presented in Figure 5. The values of C_S^{-1} calculated from the $\pi-A$ isotherms corresponded to the LC state of SM monolayers and were considerably lower than values observed at 30 mN/m for DPPC. It is also corroborated by the fact that the GIXD intensity of the Bragg peaks measured for SM is lower than the measured for DPPC. Curve 1 of the Figure 5a presents the Bragg peak for the SM monolayer spread on pure water. In contrast to DPPC, there is only one peak centered at $Q_{xy} = 1.463$ Å^{-1}. The presence of one Bragg peak is characteristic for the hexagonal 2D lattice, although the presence of a small shoulder on the lower Q_{xy} side of the peak can suggest a small distortion from the hexagonal ordering. The period of the primitive hexagonal unit cell is $a_H = 4.961$, and the L_{xy} in-plane coherence length was calculated to be 60 Å (a four times lower value than for DPPC along the (1,−1) crystallographic direction), so the average number of the molecules in the ordered SM domains can be estimated to be ∼70. The Bragg rod (curve 1 in Figure 5b) has its maximum at the horizon (0 Å^{-1}) but decays slowly with increasing Q_z values. The extended shape of the Bragg rod may suggest that it is a superposition of two Bragg rods, the first one with the maximum situated at ∼0 Å^{-1} and the second with the maximum at ca. 0.4 Å^{-1}. The fitting procedure of the Bragg rod revealed that the Bragg rod calculated in the (1−1) crystallographic direction does not overlap with the Bragg rod calculated in the (01, 10) directions. Therefore, a moderate tilt of the alkyl chains of ca. 15° was postulated for the SM alkyl chains in the monolayer. The L_z was calculated to be 15.5 Å. Taking into consideration the fact that the alkyl chain of 15 carbon atoms has a length of 19.1 Å and its projection on the z axis at a tilt angle of 15° is 18.4 Å, it is clear that not all carbon atoms of SM alkyl chains scatter X-rays coherently. This can originate from the fact that the length of both SM alkyl chains is not identical: the palmitic acid chain is longer (by about 2 C atoms) than the sphingosine one, and the terminal ethyl group of the palmitate chain is less confined. Therefore, its thermal movements may be considerable, which results in disordering and a shorter observed coherence length L_z of the scattering chain. The Bragg peaks observed for SM on $Hg(NO_3)_2$ and $HgCl_2$ solutions differ considerably from the peak measured on pure water: their intensity is lower, the peak shape is less symmetrical, and the peaks are visibly broader than on pure H_2O. Moreover, the Bragg peaks measured on mercury salts are centered at lower Q_{xy} values than on water. This trend is more pronounced for $HgCl_2$ than for $Hg(NO_3)_2$, leading to the increase of the a_H period of the primitive hexagonal unit cell from 4.961 Å on pure water to 5.273 Å on $HgCl_2$ containing subphase. The change in the peak position corresponds to the increase of the average area per molecule from 42.64 Å^2 on water to 48.15 Å^2 on $HgCl_2$. The smaller intensity of the X-ray diffraction on the mercury salt solutions results in the decrease in the in-plane coherence L_{xy} value from 60 Å on water to 47 Å on $Hg(NO_3)_2$ solution and 35 Å^2 on $HgCl_2$ solutions. The Bragg rod intensity distribution (Figure 5b) is also changed on the mercury salts as compared with the data measured on pure water. Although the rods have a maxima at ∼0 Å^{-1}, the shapes of the $I(Q_z)$ curves are different. Our fitting showed that the intensity distribution along the Bragg rods cannot be modeled as a superposition of the Bragg rods of tilted molecules. The L_z coherence lengths of the molecules are very short. The coherence length L_z decreases from a value of 15.5 Å observed on pure water to 12.7 Å on $Hg(NO_3)_2$ to only 10.24 Å on $HgCl_2$-containing subphases. Since the length of 15 C chain in the all-trans conformation is 19.1 Å, the low L_z values suggests a high degree of disorder introduced to the SM monolayers by mercuty salts, especially evident in the case of $HgCl_2$. The considerable changes of L_z can be caused by different factors: nonstoichiometric interactions of the headgroups with mercury ions, lowering the in-plane ordering, protrusions of the SM molecules into the aqueous subphase due to the complexation of mercury ions, which can cause undulation and roughness increase of the disordered monolayers. Different immersion of the neighboring SM molecules into the subphase can cause a decreasing of the van der Waals interactions of their alkyl chain termini and, in consequence, lead to an increase of the disordering of their terminal parts.

The reflectivity curves measured for SM on different subphases are presented in Figure 6. In contrast to the DPPC case, differences in the XR curves caused by the presence of mercury ions are clearly noticeable. The intensity of the XR minimum centered at ca. 0.25 Å^{-1} becomes progressively shallower when measured on the subphases containing $Hg(NO_3)_2$ and $HgCl_2$ salts. The reflectivity curves were fitted using the Parrat algorithm, and the SLD was modeled applying the two-box approximation. The scheme of the division of the SM molecules onto two boxes is shown in the formulas in Figure 7. The best fit of the reflectivity curves was obtained when the double C−C bond in the sphingosine backbone was kept in the headgroup box, while the 15 C alkyl chain of palmitic acid and 13 C chain of sphingosine were closed in the second box. The fitting parameters are showed in Table 2. The parameters obtained for the SM on pure aqueous subphase are very similar to the parameters obtained for the $Hg(NO_3)_2$ solution. The number of electrons in the headgroup box suggests that 2−2.5 water molecules are hydrating the headgroup region. The lengths of the hydrophobic chain estimated by the XR technique are very similar to the L_z value obtained from the GIXD results. The lack of significant differences in the number of electrons in the headgroup region between the monolayers on H_2O and

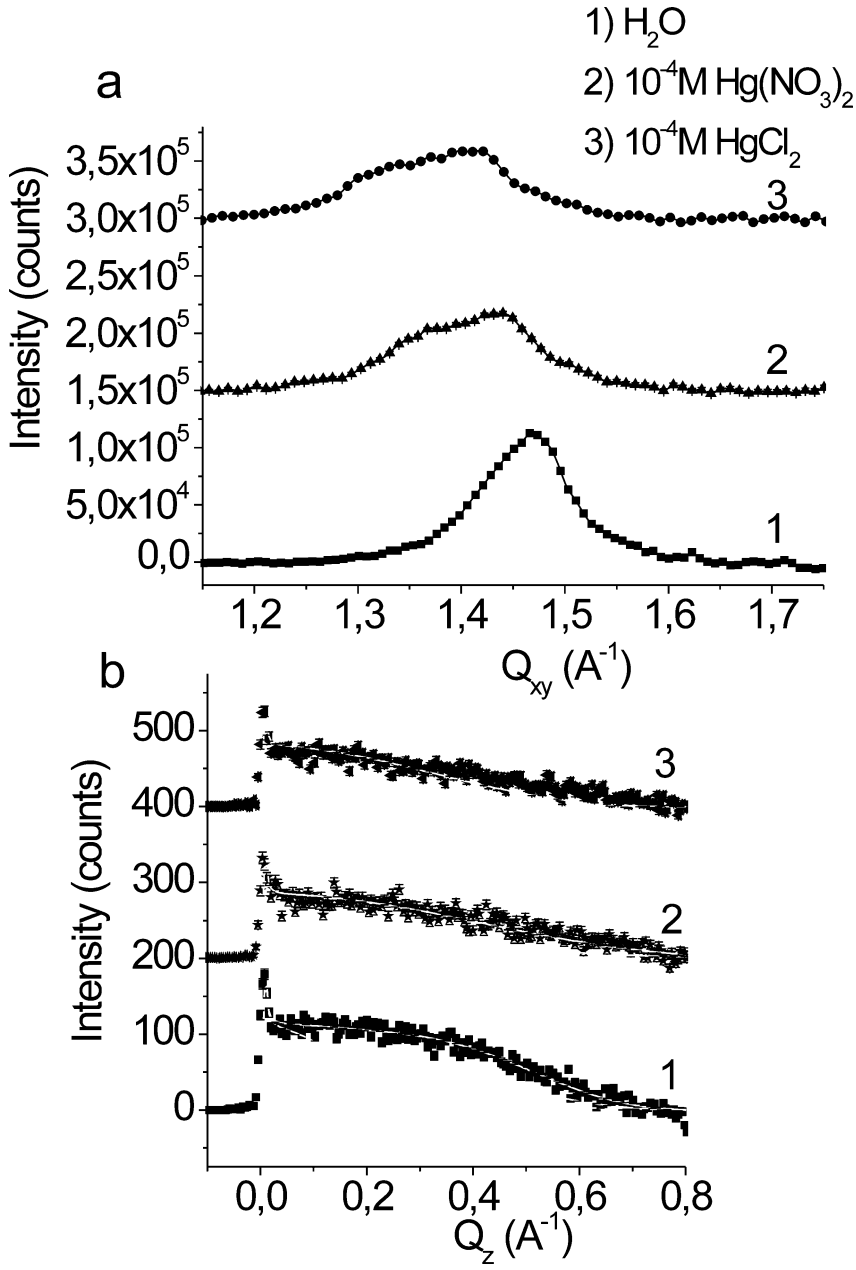

Figure 5. Background-subtracted Bragg peaks (a) and corresponding Bragg rods (b) from GIXD experiment for SM monolayers compressed to 30 mN/m. The Bragg rods were fitted by approximating the scattering unit of the molecule by a cylinder of constant electron density.[35] The Bragg peaks and rods measured on $Hg(NO_3)_2$ and $HgCl_2$ have been offset vertically for clarity.

$Hg(NO_3)_2$ solution suggest that there are no mercury ions permanently complexed to the SM headgroup.

In the case of $HgCl_2$ solution, the situation is different. The best-fit model indicates that there are 220 electrons in the headgroup box, i.e., 56 electrons more than in SM headgroup when spread on pure water. The $HgCl_2$ possesses 114 electrons, so the 56 additional electrons suggests that one molecule of mercury salt is complexed with two molecules of SM. In Figure 7b we proposed a model in which a 2:1 complex is formed. This is probably a limiting case, when all of the excess 56 e^- can be ascribed to the presence of $HgCl_2$ molecules. Most likely the number of $HgCl_2$ molecules is lower and some of the excess electrons can belong to the hydrating water molecules.

Finally, we would like to discuss the X-ray data collected for the investigated one-chain phospholipid, lyso-PC. The values of compression moduli for this compound are lower than 100, proving an expanded character of its monolayers. Such lack of in-plane order was observed in the GIXD experiments. It was impossible to measure reliable data due to extremely weak X-ray diffraction regardless of the applied subphase. The XR curves collected for lyso-PC on the three investigated subphases are presented in Figure 8.

The reflectivity curves were fitted applying the Parrat algorithm.[41] The structural models obtained for the best fits are shown in Figure 9, and the numerical values are summarized in Table 2. Similarly to DPPC and SM, the simplest two-box parametrization was applied. As can be noticed from Table 2, the thickness of the box corresponding to the alkyl chain of lyso-PC (ca. 11 Å) is very small. In our studies we used the octadecyl-lyso-PC, which contains 17 C atoms. Assuming the all-trans conformation, the length of the alkyl chain should be 21.7 Å. The small thickness of the region corresponding to the alkyl tails can be explained by immersion of the molecule in the water subphase or disordering of the alkyl chains due to

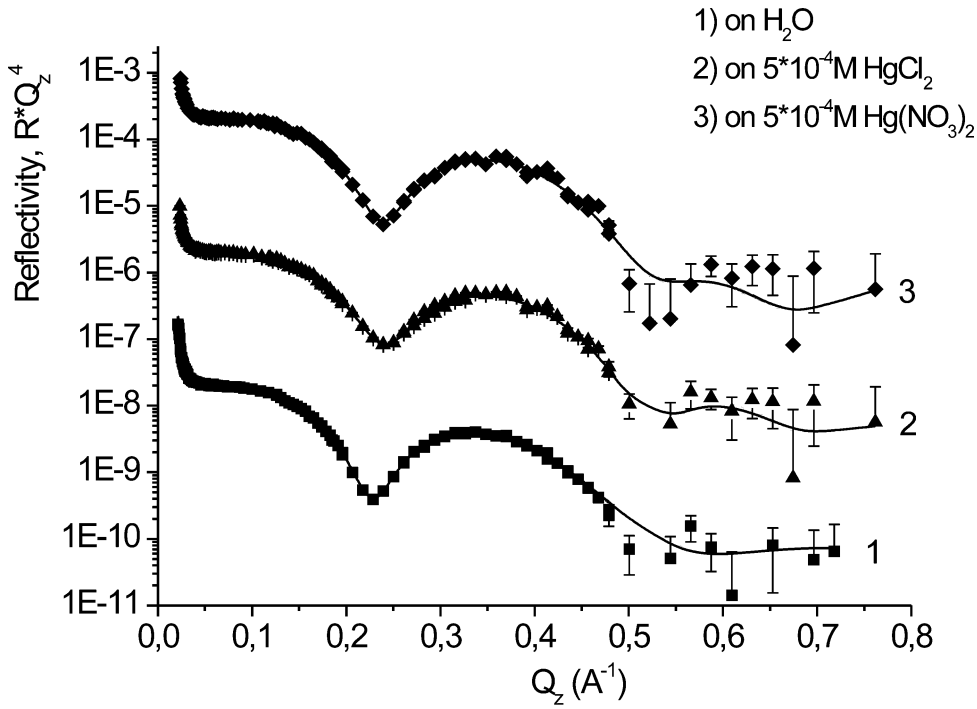

Figure 6. XR curves measured for SM monolayers with and without the mercury salts. The curves measured for the monolayers spread on the subphases containing mercury salts were offset for clarity. All XR curves were multiplied by Q_z^4 to account for the Q_z^{-4} dependence of the reflectivity due to Fresnel's law.

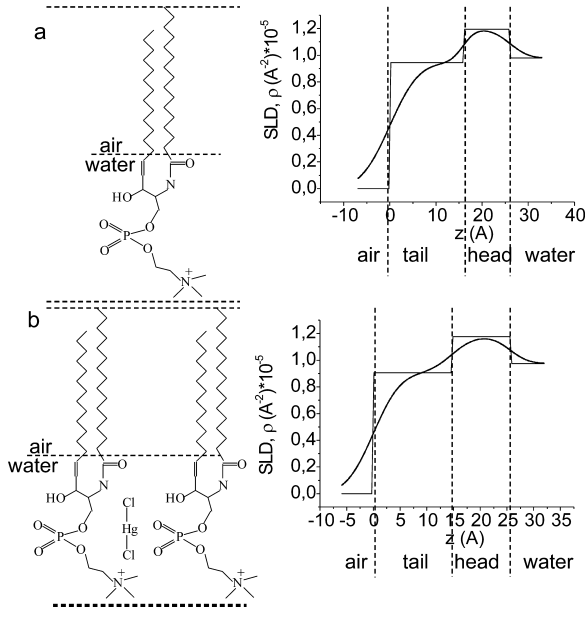

Figure 7. Profiles of the electron density for the SM monolayers obtained from the best fits of the reflectivity curves: (a) on pure water and (b) on 10^{-4} M $HgCl_2$ solution. Dashed lines illustrate the division of the molecule into two boxes of homogeneous electron density. Structure in panel b illustrates the SLD distribution with and without roughness. The fitting parameters are summarized in Table 2.

the gauche defects. Assuming a molecular tilt of 35°, characteristic for DPPC, 11 Å is a projection on the z axis of a fragment of alkyl chain containing 11 C atoms (14 Å × cos(35°)). The remaining 6-atom fragment is penetrated by water molecules and in our model was placed in the second box, containing the headgroup. The presence of a gauche conformation in the alkyl chains of the lyso-PC molecules is probable, especially in the part immersed in water; therefore, in Figure 9 we draw one gauche defect. It should be underlined that similar to the DPPC and the SM cases, the electron density obtained for the lyso-

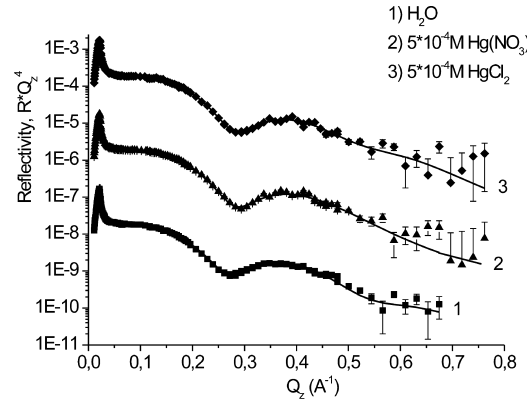

Figure 8. XR data for lyso-PC measured on pure water and the subphase containing different Hg salts. All XR curves were multiplied by Q_z^4 to account for the Q_z^{-4} dependence of the reflectivity due to the Fresnel law and offset for clarity.

PC headgroup was very similar on pure water and on the $Hg(NO_3)_2$ solution. The number of electrons in the headgroup region exceeds by ~20 the number of e^- as calculated from the chemical formula, indicating the presence of two hydration water molecules. The situation for the solution of $HgCl_2$ is pronouncedly different than in the two previous cases. The obtained number of electrons in the headgroup box is 311, which is 111 electrons more than in the headgroup region of lyso-PC on pure water. Taking into consideration that $HgCl_2$ has 114 e^-, it is visible that a considerable amount of mercury chloride was complexed by the lyso-PC headgroup. Therefore, we can postulate a 1:1 complex as illustrated in Figure 9b. It is also important to note that in the structural models constructed for lyso-PC on the solution the number of electrons in the alkyl tail box was 89, which can indicate that in the presence of $HgCl_2$ one additional $-CH_2-$ group of the alkyl chain is immersed in the aqueous subphase.

The investigated mercury salts at concentrations of 5×10^{-4} M does not change the organization of monolayers of DPPG

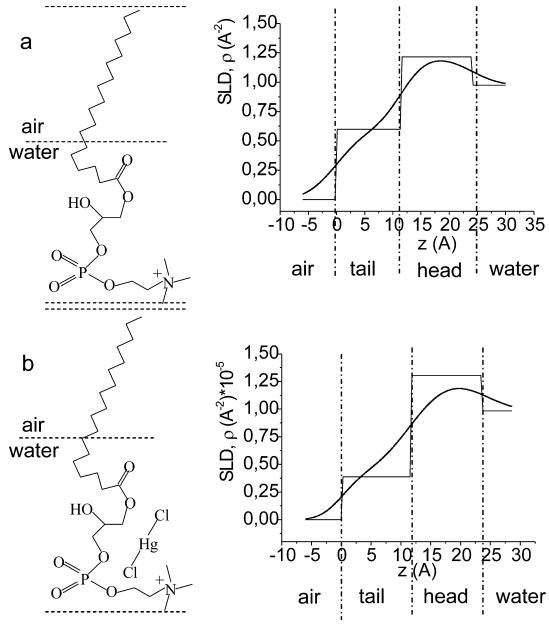

Figure 9. Profiles of the SLD for the lyso-PC monolayers obtained for the best fits of the reflectivity curves shown in Figure 8: (a) on pure water and (b) on 10^{-4} M $HgCl_2$ aqueous solution. Dashed lines illustrate the division of the molecules into boxes of homogeneous electron density. The stairlike profile plot illustrates the SLD distribution without roughness, and the smooth curve is the profile with the interfacial roughness applied. The values of the fitting parameters are shown in Table 2.

and DPPC. On the basis of the XR data, it can be stated that the electron density distribution of the DPPC and DPPG monolayers was not changed by the presence of mercury salts. This means that mercury ions are not permanently complexed by the headgroups of these lipids. The lipids formed very well organized, solid-like monolayers with a long-range in-plane order, reflected in very low compressibility (high C_S^{-1} value). The high degree of packing of the alkyl chains is also affecting the order of the headgroups. Dense packing of the headgroups limits the possible contact of the donor atoms with mercury ions and impairs the possibility of complex formation. The situation is different for lipids forming more expanded and more compressible monolayers. The tails of SM are less ordered than the tails of DPPC, which influences the organization of the headgroup and makes the headgroup−mercury salts interaction more favorable. This effect was observed in our studies. Lyso-PC is a phospholipid possessing only one alkyl chain attached to a relatively large headgroup (as far as the cross-section areas of both moieties are compared). The monolayers are in the liquid-expanded state and even at 30 mN/m are not ordered enough to diffract synchrotron radiation in the GIXD experiment. The headgroup of lyso-PC has much more conformational freedom as compared to the lipids with the headgroups attached to a double-chain lipid. Therefore, the interactions of the headgroup with mercury salts of one-chain phospholipid should be stronger than in the case of a double-chain compound. The second important fact which should be underlined is the difference between $Hg(NO_3)_2$ and $HgCl_2$, as only the latter compound was observed to interact noticeably with SM and lyso-PC. Similar trends were observed by us for monolayers of simple one-chain surfactants.[28] Most dangerous for living organisms are those compounds of mercury, which do not dissociate in the aqueous environment, liberating hydrated mercury(II) cations.[9] Therefore, mercury chloride is a much more appropriate model of the mercury compounds present in living organisms than $Hg(NO_3)_2$ or other oxacid salts of mercury. It is well known that mercury compounds are accumulated in the brain and can easily access this organ crossing the blood−brain barrier.[1,2] In neurons, the amount of SM in the cell membranes is noticeably higher than in other cell lines, and moreover, SM is also the main lipid component of the myeline shell. Our experiments, in which we show the propensity of SM to complex mercury ions, which differtiates it from other double-chain phospholipids, shed new light on the well-known problem of the accumulation of mercury in the nervous system.

Conclusions

In our studies we investigated the influence of mercury salts dissolved in the aqueous subphase on the behavior of Langmuir monolayers of selected phospholipids. The interaction depends both on the fluidity of phospholipid monolayer as well as on the type of mercury salt. Double-chain phospholipids of a low compressibility, such as DPPG and DPPC, do not permanently complex mercury ions as no accumulation of mercury salts in the monolayer was observed. This was interpreted as being due to a high degree of order in these films, i.e., low conformational freedom of the monolayer headgroups. The phospholipids forming less crystalline (more compressible) monolayers, such as SM and lyso-PC, can complex permanently and accumulate mercury ions at the water/air interface. However, differences appear regarding the type of mercury salt. Lipophilic, weakly dissociating in water hydracid salts of mercury, like $HgCl_2$, are stronger complexed than oxacid mercury salts. Therefore, $HgCl_2$ seems to be a better model of mercury-containing compounds present in a living organism than $Hg(NO_3)_2$. The observed differences between DPPC and SM, compounds which have very similar headgroups, shed new light on the problem of mercury accumulation in living organisms. Our experiments proved that synchrotron X-ray methods are very valuable tools in studies of the mercury interaction with cell membrane lipids.

Acknowledgment. M.B. and P.D.-Ł. are grateful for financial support from the Polish Ministry of Science and Higher Education (Grant No. N N204 323937). The work benefited from the use of the Lujan Neutron Scattering Center at LANCE funded by the DOE Office of Basic Energy Sciences and Los Alamos National Laboratory under DOE Contract DE-AC52-06NA25396.

References and Notes

(1) Clarkson, T. W.; Magos, L.; Myers, G. J. *New Engl. J. Med.* **2003**, *349*, 1731–1737.
(2) Gochfeld, M. *Ecotoxicol. Environ. Saf.* **2003**, *56*, 174–179.
(3) Harris, H. H.; Pickering, I. J.; George, G. N. *Science* **2003**, *301*, 1203–1203.
(4) Risher, J. F.; Nickle, R. A.; Amler, S. N. *Int. J. Hyg. Environ. Health* **2003**, *206*, 371–379.
(5) Gad, S. C. *Encyclopedia of Toxicology*; Elsevier: Oxford, 2005; Vol. 3, pp 36−39.
(6) Son, M. H.; Kang, K. W.; Lee, C. H.; Kim, S. G. *Toxicol. Lett.* **2001**, *121*, 45–55.
(7) Rooney, J. P. K. *Toxicol.* **2007**, *234*, 145–156.
(8) Woods, J. S.; Echeverria, D.; Heyer, N. J.; Simmonds, P. L.; Wilkerson, J.; Farin, F. M. *Toxicol. Appl. Pharmacol.* **2005**, *206*, 113–120.
(9) Bridges, C. C.; Zalups, R. K. *Toxicol. Appl. Pharmacol.* **2005**, *204*, 274–308.
(10) Suvalsky, M.; Ungerer, B.; Villena, F.; Cuevas, F.; Sotomayor, C. P. *J. Inorg. Biochem.* **2000**, *81*, 267–273.
(11) Zolla, L.; Lupidi, G.; Bellelli, A.; Amiconi, G. *Biochim. Biophys. Acta* **1997**, *1328*, 273–280.
(12) Pribush, A.; Meyerstein, D.; Meyerstein, N. *Biochim. Biophys. Acta* **2002**, *1558*, 119–132.
(13) Le, M. T.; Gailer, J.; Prenner, E. J. *Biometals* **2009**, *22*, 261–274.

(14) Girault, L.; Lemaire, P.; Boudou, A.; Debouzy, J. C.; Dufourc, E. J. *Eur. Biophys. J.* **1996**, *24*, 413–421.
(15) Girault, L.; Boudou, A.; Dufourc, E. J. *Biochim. Biophys. Acta* **1997**, *1325*, 250–262.
(16) Collin-Hansen, C.; Andersen, R. A.; Steinnes, E. *Mycol. Res.* **2005**, *109*, 1386–1396.
(17) Mazerik, J.; Mikkilineni, H.; Kuppusamy, V. A.; Steinhour, E.; Peltz, A.; Marsh, C. B.; Kuppusamy, P.; Parinandi, N. L. *Toxicol. Mech. Methods* **2007**, *17*, 541–557.
(18) Cho, U. H.; Park, J. O. *Plant Sci.* **2000**, *156*, 1–9.
(19) Berntssen, M. H. G.; Aatland, A.; Handy, R. D. *Aquat. Toxicol.* **2003**, *65*, 55–72.
(20) Silbergeld, E. K.; Devine, P. J. *Fuel Process. Technol.* **2000**, *65*−*66*, 35–42.
(21) Warfvinge, K.; Bruun, A. *Toxicology* **1996**, *107*, 189–200.
(22) Aduayom, I; Denizeau, F.; Jumarie, C. *Cell Biol. Toxicol.* **2005**, *21*, 163–179.
(23) Brockman, H. *Curr. Opin. Struct. Biol.* **1999**, *9*, 438–443.
(24) Rosetti, C. M.; Maggio, B.; Oliveira, R. G. *Biochim. Biophys. Acta* **2008**, *1778*, 1665–1675.
(25) Lee, K. Y. C.; Majewski, J.; Kuhl, T. L.; Howes, P. B.; Kjaer, K.; Lipp, M. M.; Waring, A. J.; Zasadzinski, J. A.; Smith, G. S. *Biophys. J.* **2001**, *81*, 572–585.
(26) Schionning, J. D.; Larsen, J. O.; Eide, R. *Acta Neuropathol.* **1998**, *96*, 185–190.
(27) Sabolić, I. *Nephron Physiol.* **2006**, *104*, 107–114.
(28) Broniatowski, M.; Dynarowicz-Łątka, P. *J. Phys. Chem. B* **2009**, *113*, 4275–4283.
(29) Vaknin, D. *J. Am. Chem. Soc.* **2003**, *125*, 1313–1318.
(30) Miller, C. E.; Majewski, J.; Kuhl, T. L. *Colloid. Surfaces A: Physicochem. Eng. Aspects* **2006**, *284*−*285*, 434–439.
(31) Majerowicz, M.; Waring, A. J.; Wen, S.; Bringezu, F. *J. Phys. Chem. B* **2007**, *111*, 3813–3821.
(32) Wagner, K.; Brezesinski, G. *Chem. Phys. Lipids* **2007**, *145*, 119–127.
(33) Schalke, M.; Lösche, M. *Adv. Colloid Interface Sci.* **2000**, *28*, 243–274.
(34) Majewski, J.; Popovitz-Biro, R.; Bouwman, W.; Kjaer, K. *Chem.*−*Eur. J.* **1995**, *1*, 302–309.
(35) Jensen, T. R.; Kjaer, K. *Novel Methods to Study Interfacial Monolayers*; Mobius, D., Miller, R., Eds.; Elsevier: Amsterdam, 2001; Vol. 11, pp 205−254.
(36) Born, M.; Wolf, E. *Principles of Optics*; Pergamon Press: Oxford, 1984.
(37) Wu, D. G.; Malec, A. D.; Majewski, J.; Majda, M. *Electrochim. Acta* **2006**, *51*, 2237–2246.
(38) Kjaer, K. *Physica B* **1994**, *198*, 100–109.
(39) Braslau, A.; Deutsch, M.; Pershan, P. S.; Weiss, A. H.; Als-Nielsen, J.; Bohr, J. *Phys. Rev. Lett.* **1985**, *54*, 114–117.
(40) Pershan, P. S. *Faraday Discuss. Chem. Soc.* **1990**, *89*, 231–245.
(41) Parrat, L. G. *Phys. Rev.* **1954**, *95*, 359–369.
(42) Neville, F.; Ishitsuka, Y.; Hodges, C. S.; Konovalov, O.; Waring, A. J.; Lehrer, R.; Lee, K. Y. C.; Gidalevitz, D. *Soft Matter* **2008**, *4*, 1665–1674.
(43) Bu, W.; Flores, K.; Pleasants, J.; Vaknin, D. *Langmuir* **2009**, *25*, 1068–1073.
(44) Als-Nielsen, J.; Jacquemain, D.; Kjaer, K.; Leveiller, F.; Lahav, M.; Leiserowitz, L. *Phys. Rep.* **1994**, *246*, 251–313.
(45) Grant, G. J. *Encyclopedia of Inorganic Chemistry*; J. Wiley &Sons: New York, 1994; pp 2136−2145.
(46) Gaines, G. L., Jr. *Insoluble monolayers at liquid-gas interface*; Interscience Publishers: New York, 1966.
(47) Pedersen, J. S.; Hamley, I. W. *J. Appl. Crystallogr.* **1994**, *27*, 36–49.
(48) Brezesinski, G.; Vollhardt, D.; Iimura, K.; Cölfen, H. *J. Phys. Chem. C* **2008**, *112*, 15777–15783.
(49) Ege, L.; Ratajczak, M.; Majewski, J.; Kjaer, K.; Lee, K. Y. C. *Biophys. J.* **2006**, *91*, L01–L03.
(50) Pascher, I.; Sundell, S.; Eibl, H.; Harlos, K. *Chem. Phys. Lipids* **1986**, *39*, 53–64.

JP101668N